BMA Gripper: Bistable Multimode Adaptive Gripper Enabled by a Spring-Latch Mechanism

Tao Liao, Houde Liu, Chongkun Xia, *Member, IEEE*, Shoujie Li, *Member, IEEE*, Xueqian Wang, *Member, IEEE*, and Bin Liang, *Senior Member, IEEE*

***Abstract*—Bistable grasping devices exhibit high maneuverability and rapid responsiveness; however, existing bistable grippers often lack the capability for active adjustment of triggering forces and effective interaction with the environment during grasping. Inspired by the zebra mantis shrimp, this article proposes a bistable, multimode, and adaptive gripper named bistable multimode adaptive gripper (BMA) gripper. Through a bioinspired design of a multimode bistable actuator and underactuated fingers with modular fingertips, the proposed gripper achieves rapid grasping across diverse scenarios. A series of experiments were conducted to evaluate the performance and functionality of the BMA gripper. Experimental results demonstrate that the gripper can operate in three distinct grasping modes: fully active, active bistable, and passive bistable grasping, effectively interacting with the environment to achieve adaptive grasping. In the bistable grasping mode, the gripper requires a minimal energy of only 0.412 mJ for state transition and can switch from the open state to the closed state in as short as 0.116 s. In addition, the gripper achieves a maximum gripping force of 68.4 N at a gripping distance of 120 mm. These results confirm the significant potential of the BMA gripper for high-speed adaptive grasping tasks in various application scenarios.**

***Index Terms*—Bistable structure, dynamic capture, mode switching, reprogrammable, two-finger gripper.**

Received 12 November 2024; revised 21 March 2025 and 9 June 2025; accepted 17 September 2025. Recommended by Technical Editor Mokrane Boudaoud and Senior Editor C. Clévy This work was supported in part by the Dreams Foundation of Jianghuai Advance Technology Center under Grant 2023-ZM01Z005, in part by the National Natural Science Foundation of China under Grant 62203260 and Grant 92248304, in part by the Shenzhen Science Fund for Distinguished Young Scholars under Grant RCJC20210706091946001, and in part by the Guangdong Basic and Applied Basic Research Foundation under Grant 2023A1515011773. *(Corresponding author: Houde Liu.)*

Tao Liao, Shoujie Li, and Xueqian Wang are with Tsinghua Shenzhen International Graduate School, Tsinghua University, Shenzhen 518055, China (e-mail: liaot23@mails.tsinghua.edu.cn; lsj20@mails.tsinghua.edu.cn; wang.xq@sz.tsinghua.edu.cn).

Houde Liu is with Tsinghua Shenzhen International Graduate School, Tsinghua University, Shenzhen 518055, China, and also with Jianghuai Advance Technology Center, Hefei 230000, China (e-mail: liu.hd@sz.tsinghua.edu.cn).

Chongkun Xia is with the School of Advanced Manufacturing, Sun Yat-Sen University, Shenzhen 518055, China (e-mail: xiachk5@mail.sysu.edu.cn).

Bin Liang is with the Navigation and Control Research Center, Department of Automation, Tsinghua University, Beijing 100084, China (e-mail: bliang@tsinghua.edu.cn).

This article has supplementary material provided by the authors and color versions of one or more figures available at https://doi.org/10.1109/TMECH.2025.3612897.

Digital Object Identifier 10.1109/TMECH.2025.3612897

I. Introduction

As A fundamental function of animals, grasping plays a crucial role in interactions with the natural world [1], [2]. Grasping mechanisms have been studied for over 60 years in academia, yet actively driven parallel grippers remain the standard in real-world applications due to their ability to generate substantial grip forces based on the torque provided by their actuators [3]. However, these grippers face significant limitations, such as slow grasping speeds, challenges in capturing high-dynamic objects, and difficulties in interacting with complex environments [4].

In contrast, numerous organisms in nature have evolved bistable structures to enhance their survival. Examples include the flexible actuators in Venus flytrap leaves [5], the rapid beak closure of hummingbirds to catch flying insects [6], the fast folding and locking of earwig wings [7], and the lightning-fast strikes of the mantis shrimp's hunting limbs [8]. These bistable structures exhibit unparalleled advantages in rapid response and force amplification. By setting specific triggering conditions, bistable mechanisms enable rapid transitions between two stable states, releasing significant amounts of stored strain energy in an extremely short time frame, thereby enhancing grasping speed and force output [9]. Moreover, bistable mechanisms inherently maintain their shape after transitioning, eliminating the need for continuous actuation and reducing energy consumption [10].

In recent years, considerable research has focused on applying bistable structures in grasping devices. Based on the energy transition mechanisms, these devices can be categorized into origami-inspired designs [11], [12], [13], flexible material-based structures [14], [15], [16], rigid deformation structures [17], [18], and energy-assisted designs [19], [20]. However, most existing studies have been limited to a single, passive triggering mode, where any external stimulus instantly initiates closure. This limitation prevents active control over the triggering of bistable structures and restricts their ability to adapt to diverse grasping scenarios.

In addition, the sensitivity and transition speed of bistable structures are largely determined by their preset structural parameters and material properties [21], [22]. Once fabricated, these properties become fixed and unmodifiable [23]. Moreover, during bistable transitions, current devices often struggle with

environmental interactions—unintended external interference can prevent successful closure. Achieving fine-tuned, postfabrication control over triggering sensitivity and transition speed while ensuring reliable environmental interaction during grasping remains a significant challenge [24], [25].

Biological structures and behaviors have long inspired robotic design. Notably, the zebra mantis shrimp features a hunting appendage equipped with a unique spring-latch mechanism that enables bistable triggering. This appendage extends rapidly and adaptively grasps prey, demonstrating a high degree of environmental adaptability and fast grasping efficiency [26]. Inspired by this physiological structure and predation mechanism, we propose the bistable multimode adaptive gripper (BMA) Gripper—a bistable, multimodal, and adaptive gripper designed for high-speed, adaptive grasping of both static and dynamic objects. The main contributions of this work are as follows.

1) The proposed BMA Gripper leverages a bistable structure to enable rapid capture of static and high-dynamic objects, with reprogrammable trigger sensitivity and grasping speed without increasing mechanical complexity.
2) The proposed BMA Gripper can freely switch between three working modes and adapt to different grasping tasks by manually changing its fingertips.
3) The proposed BMA Gripper is capable of rapid grasping during environmental interaction, reducing dependency on detailed target and environmental information, and avoiding the need for complex planning algorithms.

II. Design of the Grasping and Workflow

A. Bioinspired Design

The zebra mantis shrimp, known as "Brawler of the Seafloor," exhibits exceptionally powerful strikes and ultra-fast predatory responses [27]. As shown in Fig. 1(a), it possesses two hunting limbs, each with an agile dual-joint structure. This configuration allows strike-and-grasp or direct envelopment strategies, depending on prey size [8], [28]. In addition, during predation, the shrimp's forelimbs can accelerate from rest to over 20 m/s in less than 3 ms, a capability closely associated with its spring-latch mechanism embedded within the retraction muscles of the hunting limbs. In the preparation phase, forelimbs retract, storing elastic potential energy in muscle tissues. This energy is then rapidly released to propel the limbs forward at remarkable speed. Leveraging this specialized morphology, the shrimp can capture even evasive prey with instantaneous strikes [30].

As shown in Fig. 1(b), zebra mantis shrimp's hunting appendages primarily comprise three key physiological structures: a spring tendon, a latch tendon, and a double-joint mechanism. This tendon-driven system exhibits bistable characteristics. During hunting preparation, the latch tendon contracts, stretching the spring tendon located opposite the first flexible joint. Subsequently, the latch tendon is locked, maintaining the limb in a "latch-locked" configuration—defined as the first stable state. Upon attack initiation, the latch rapidly releases, allowing appendages to extend swiftly under spring tendon force, striking prey and transitioning into the second stable state. After impact, prey is adaptively enveloped by the second flexible joint and then retracted through the first joint, completing a rapid strike-and-retrieval sequence, as shown in Fig. 1(c). Furthermore, as demonstrated in Fig. 1(c), zebra mantis shrimp adjusts its predatory strategy based on prey size. For larger prey, it performs a strike followed by envelopment and retrieval; for smaller prey, it applies a direct enveloping grasp without a preceding strike.

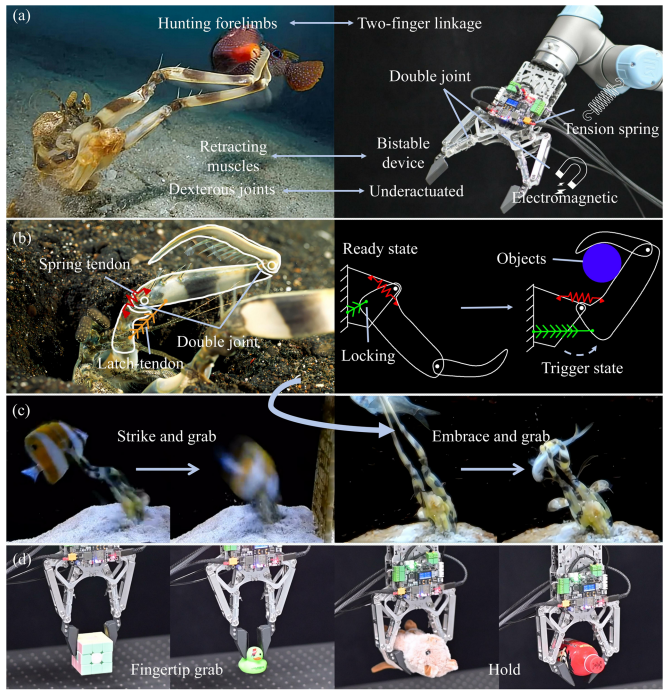

Fig. 1. Bioinspired bistable, multimode, adaptive gripper based on the zebra mantis shrimp. (a) Zebra mantis shrimp employs dexterous double joints and retractor muscles to achieve high-speed hunting and adaptive grasping; the proposed BMA gripper achieves rapid adaptive grasping through an underactuated double-joint linkage and bistable mechanism. (b) Physiological structure of the zebra mantis shrimp's predatory limb, including spring-latch tendons and double joints. (c) Operational process mimicking the zebra mantis shrimp's predatory limb, featuring striking grasp and enveloping grasp. (d) Two grasping modes of the BMA gripper: fingertip grasping and enveloping grasping, corresponding, respectively, to the mantis shrimp's striking and direct enveloping strategies for prey of different sizes.

Inspired by the physiological structure and predation mechanisms of zebra mantis shrimp's hunting appendages, we propose a two-fingered gripper with integrated bistable and adaptive capabilities, termed the BMA gripper, as shown in Fig. 2. This design primarily comprises an electromagnetic-pneumatic actuator and an underactuated linkage claw mechanism. By employing electromagnets and tension springs to store and rapidly release energy, the gripper achieves high-speed extension for object grasping, effectively emulating the spring-latch mechanism and adaptive predation behavior observed in zebra mantis shrimp.

As shown in Fig. 1(d), the underactuated linkage claw supports two distinct grasping modes: fingertip grasping for smaller objects and adaptive enveloping grasping via inner surfaces for larger objects. Moreover, BMA gripper incorporates a modular fingertip design and achieves multiple operational modes by adjusting activation intervals of its electromagnetic-pneumatic actuator, enabling effective adaptation to diverse grasping tasks.

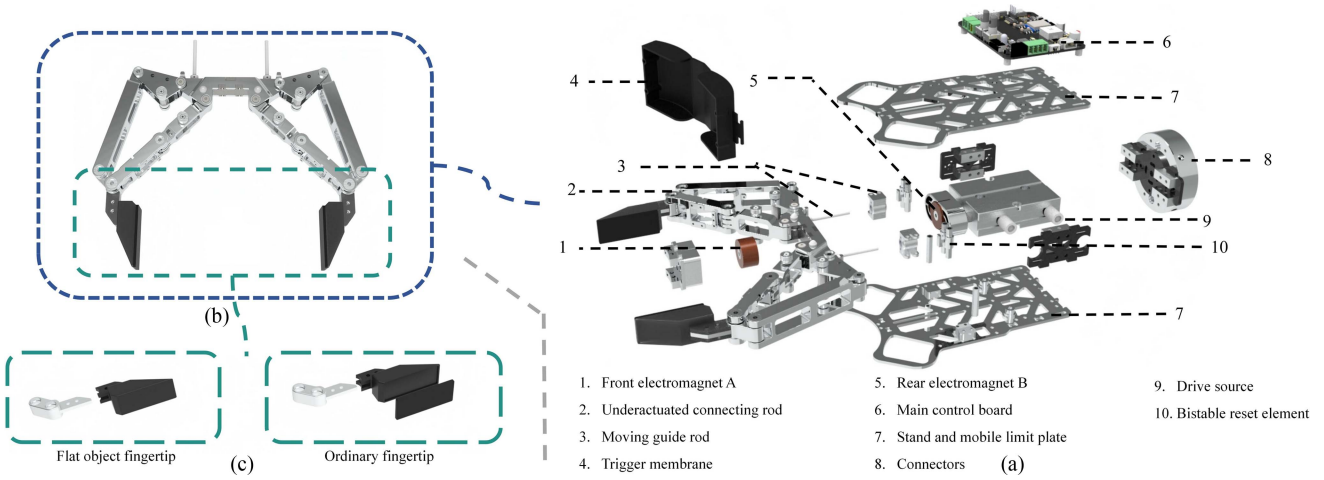

Fig. 2. Overview of the violet gripper inspired by the zebra mantis shrimp. (a) Exploded view of the violet end-effector. (b) Structure of the underactuated linkage gripper mechanism. (c) Modular fingertip design with decomposition view.

This adaptability is analogous to the biological strategy adjustments observed in the zebra mantis shrimp when capturing prey of varying sizes. Such bioinspired implementation offers valuable insights and design principles for developing high-speed grasping systems.

B. Hunting Limb-Inspired Gripper

During the predation process of the zebra mantis shrimp, four primary phases are observed: energy storage, rapid limb extension, adaptive grasping, and retraction. Inspired by the physiological structure of its hunting limbs, we developed an underactuated linkage gripper system—comprising a six-bar underactuated mechanism and a trajectory-guiding module—to achieve functions, such as rapid extension during grasping and adaptive object engagement.

As shown in Fig. 3(a), the underactuated linkage gripper device consists of two main components: an underactuated six-bar linkage and a trajectory-guiding module. The joints of the six-bar linkage are connected via bearings, and TPU elastic bands are affixed at each linkage joint to provide restoring elastic forces that maintain the initial configuration. A tension spring (Spring 1) is mounted on the moving block to supply the energy required for rapid bistable transitions. The spring is designed with a quick-swap mechanism, allowing users to replace it with versions of different wire diameters and lengths, thereby enabling programmable control of the closing speed during state transitions. To achieve passive triggering in response to external stimuli, a modular trigger membrane made of 75 A rubber is incorporated. Rectangular slots are cut into both ends of the membrane, which is fixed at the midpoints of linkages DC and D_1C_1 using 2 mm thick metal plates. Threaded holes are provided at connection points G and G_1, ensuring secure attachment of the membrane to the linkage structure. During grasping, the gripper exhibits compliant contact behavior. This is achieved through the combined effect of a second tension spring positioned between linkages AF and AB, and two sets of

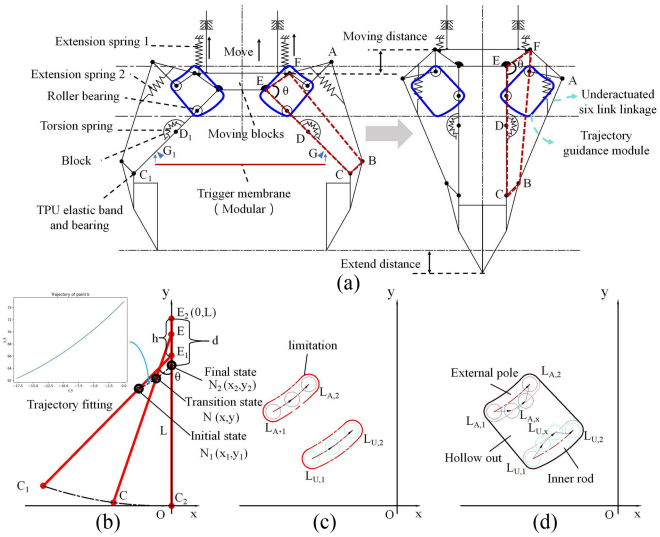

Fig. 3. (a) Overall structure of the underactuated linkage gripper in the BMA gripper, along with its two stable states: open and closed. (b) Motion diagram of link EC from open to closed in the underactuated linkage claw, and curve fitting of the roller bearing's trajectory. (c) Constraint on the link's motion trajectory set by the support and the movable limit plate, yielding a single solution. (d) Constraint on the link's motion trajectory set by the support and the movable limit plate, yielding infinite solutions when contact compliance is considered.

torsion springs located between linkages CD and DE. A blocking structure is installed at the end of linkage DE, with the torsion springs supplying an initial torque to maintain the parallel alignment between CD and DE. To realize the desired compliance and triggering behavior, the inner linkages are designed to initiate deformation when subjected to an external torque exceeding 0.14 N· m. Based on this design target, the parameters of the torsion springs are determined via inverse calculation using the following equation:

$$M = 2 \cdot \frac{E \cdot d^4 \cdot \theta}{10.8 \cdot D \cdot n}. \tag{1}$$

The parameters in the equation are defined as follows: M is the torque, E is the elastic modulus, d is the wire diameter of the torsion spring, D is the mean diameter of the spring, n is the number of effective coils, and θ is the torsion angle (initially set to 0.1745 rad to provide a preload torque for early warning). The selected torsion spring parameters must generate an initial torque of approximately 0.15 N· m under structural space constraints, ensuring that the inner compliance mechanism can be reliably triggered at the designed threshold.

In addition, the tension spring between linkages AF and AB provides outer-side compliant contact capability and cooperates with the inner torsion springs to maintain a vertical fingertip orientation. When the externally applied force transmitted along the direction of the tension spring exceeds the preset threshold, the outer compliance mechanism should be triggered to adjust the gripper posture. In this study, we set the outer triggering force threshold at 1.2 N with an initial elongation of 5 mm, and inversely derived the spring parameters using the following equation:

$$F = \frac{E \cdot d^4 \cdot \Delta L}{8 \cdot D^3 \cdot n} \tag{2}$$

where F is the tensile force, E is the elastic modulus, d is the wire diameter of the tension spring, ΔL is the elongation of the spring, D is the mean diameter, and n is the number of effective coils. The selected spring parameters must satisfy spatial constraints while generating an initial tensile force of approximately 1.25 N to ensure that the outer compliant mechanism is reliably triggered at the designated threshold.

On the other hand, due to the tension provided by the tensile spring, links AF and AB can be considered as an integrated link equivalent to link BF. To achieve forward fingertip extension during gripper closure, a floating trapezoidal four-bar linkage mechanism was designed, consisting of link EF (frame link, length 24.5 mm), link EC (driver link, length 100 mm), link FB (coupler link, length 96 mm), and link BC (output link, length 14.5 mm), precisely controlling the fingertip position. For the overall motion, the linear travel of the moving block was set to 20 mm, with a maximum finger opening distance of 140 mm to accommodate grasping of most small- to medium-sized objects.

During the transition from open to closed states, the moving block drives the gripper backward by 20 mm, while the input angle θ of the trapezoidal linkage rotates by 42°, resulting in nonlinear fingertip motion. Through motion analysis in three-dimensional modeling software, initial and final states were set, and the corresponding movement curves recorded. The resulting trajectory shown in Fig. 3(a) was generated and fitted into the model, indicating a forward fingertip extension of 22.5 mm for the proposed linkage dimensions.

To actuate the underactuated six-link mechanism for grasping tasks, we utilize the trajectory-guiding characteristics of a cam system. A roller bearing (NTBGT9-8) is mounted on the linkage, while guiding tracks are incorporated on the bracket and the sliding limiter to direct the motion of the gripper. As shown in Fig. 3(b), during the transition from open to closed states, link EC undergoes rotational motion around pivot point E and linear translation along the negative direction of the y-axis. The roller bearing's initial and final positions are denoted as N_1 and N_2, respectively, with intermediate positions represented as N. The global coordinates of point N during motion can be expressed as

$$\begin{cases} x_N(\theta) = -d\sin\theta \\ y_N(\theta) = y_E(\theta) - d\cos\theta \end{cases} \tag{3}$$

where θ is the angle between link EC and the y-axis, x_N and y_N represent the horizontal and vertical coordinates of point N, respectively, and d is the distance between the roller bearing and point E. Since the motion of link EC is driven by the moving block, point E moves linearly and uniformly along the negative y-axis; thus, its coordinate relationship can be simplified as

$$y_{E(\theta)} = L + \frac{(L-h-L)(\theta-0)}{\theta_{\max}-0} = L - \frac{h\theta}{\theta_{\max}} \tag{4}$$

where $\theta_{\max}$ represents the initial angle between link EC and the y-axis, L is the length of link EC, and h denotes the displacement of the moving block. Consequently, the simplified global coordinates of point N become

$$\begin{cases} x_N(\theta) = -d\sin(\theta) \\ y_N(\theta) = L - \frac{h\,\theta}{\theta_{\max}} - d\cos(\theta) \end{cases} \quad \theta \in [0, \theta_{\max}]. \tag{5}$$

When $\theta = \theta_{\max}$, the linkage is in the open position, and the roller bearing is at the initial position $N_1(-d\sin\theta_{\max},\ L-h-d\cos\theta_{\max})$; when $\theta = 0$, the linkage is in the closed position, and the roller bearing is at the final position $N_2(0,\ L-d)$. The trajectory defined by this parametric equation is plotted using Python and subsequently fitted onto the support bracket and movement-limiting plate, effectively guiding the gripper's movement, as shown in Fig. 3(c).

However, the trajectory shown in Fig. 3(c) is fixed, resulting in a unique solution for gripper motion. Merely constraining initial and final positions is insufficient for achieving adaptive interaction with the environment. As shown in Fig. 3(d), open spaces are intentionally created between the two roller bearings on each side, removing trajectory constraints to allow infinite possible solutions during movement. Points L_{A1}, L_{U1}, and L_{A2}, L_{U2} represent the initial and final positions of the two roller bearings, respectively, while L_{Ax} and L_{Ux} denote intermediate positions during adaptive interaction with the environment.

Based on the integration of the underactuated six-bar linkage and the trajectory-guiding module, the underactuated linkage gripper exhibits multidirectional adaptability, enabling reliable grasping without the need for precise information about the target object or surrounding environment. During gripper closure, the fingertips perform unobstructed motion consisting of a vertical extension, which allows adaptation to vertical gaps, as shown in Fig. 4(a). When horizontal contact with the environment needs to be accommodated, as shown in Fig. 4(b), the outer roller bearing follows the trajectory L_{A1}–L_{A2} shown in Fig. 3(d). For vertical direction adaptation during contact with the environment or object, as illustrated in Fig. 4(c) and (d), the inner roller bearing follows the trajectory L_{U1}–L_{U2} in Fig. 3(d).

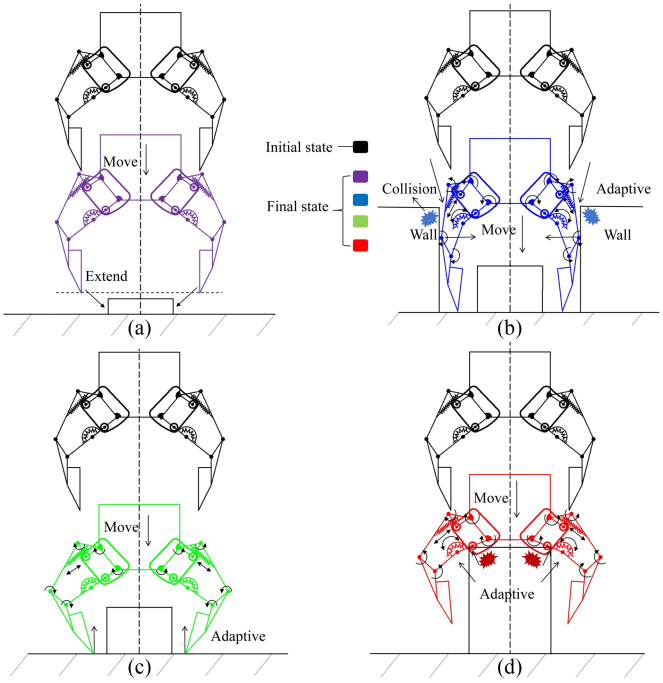

Fig. 4. Adaptive grasping modes of the underactuated linkage gripper under conditions of limited information. (a) Fingertips extend to grasp objects when vertically too distant and no horizontal contact occurs. (b) Horizontal adaptive grasping within narrow spaces. (c) Adaptive grasping through ground contact when vertically too close to the object. (d) Internal adaptive grasping for objects with unusual shapes or greater heights.

C. Actuation Inspired by Muscle Contraction

During the predation process of the zebra mantis shrimp, its hunting limbs fold and contract toward the body under active muscular drive. The muscle structure stores elastic potential energy through contraction and tension, accumulating this energy within the spring tendons of the hunting limbs via a specialized spring-latch mechanism. When the moment to strike arrives, the latch tendon suddenly relaxes, releasing the latch mechanism. The stored elastic potential energy is then instantaneously discharged, causing the hunting limbs to rapidly extend from the folded state, strike the prey, and immediately retract for capture.

In response to the specialized spring-latch mechanism within these muscles, we designed a drive unit using electromagnets and a pneumatic cylinder, endowing the BMA gripper with three operating modes: fully active grasping, active bistable grasping, and passive bistable grasping. As shown in Fig. 5, this drive unit features a moving block equipped with two iron plates at its front and rear ends to interact with two electromagnets. The moving block is further connected to a movement limit plate via tension springs, which provide the elastic potential energy for state transitions. In this drive unit, Electromagnet A, located at the front, can vary its magnetic force in both the active and passive bistable modes, thereby allowing precise control over the gripper's speed and triggering sensitivity. Meanwhile, Electromagnet B, located at the rear, supplies the magnetic force needed to counter the backward impact of the moving

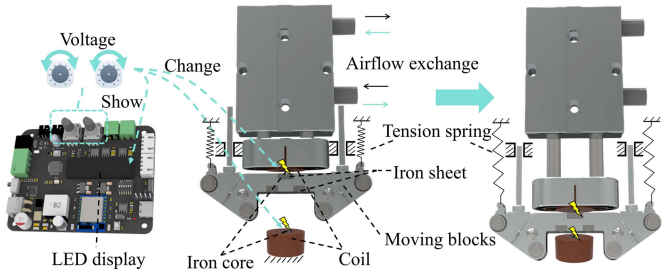

Fig. 5. Muscle contraction-inspired actuator design and electromagnetic control principles.

block during rapid closure of the jaws, preventing rebound and unintended reopening, and thus enhancing grasping stability.

The muscle-contraction-inspired drive unit occupies a space of 54 × 140 × 25 mm. It uses the STM32 G431C8T6 as its microcontroller unit (MCU), with a custom-designed PCB for control. In order to precisely regulate the voltage of the solenoid and adjust its triggering sensitivity, we employ the following voltage divider circuit principle on the PCB:

$$U_{\mathrm{OUT}} = U_{\mathrm{FB}} \times \frac{(R_{\mathrm{FB1}} + R_{\mathrm{FB2}})}{R_{\mathrm{FB1}}}. \tag{6}$$

The output voltage of the electromagnet (U_{out}) is determined by the total input voltage (U_{FB}) and the resistances (R_{FB1} and R_{FB2}). By adjusting these resistances using a potentiometer, the magnetic force of the electromagnet can be precisely controlled, thereby regulating the closure speed and trigger sensitivity of the gripper in both the active and passive bistable grasping modes (PBGMs). In addition, the voltages applied to both electromagnets are displayed in real time via a display screen. Permanent magnets are installed on both sides of Electromagnet A at the front end, which enables the BMA gripper to achieve a fixed, nonadjustable passive bistable grasp using a low-tension tensile spring (0.5 mm wire diameter, 25 mm length) when Electromagnet A is not activated. When Electromagnet A is activated, the permanent magnets and Electromagnet A jointly provide magnetic force, thereby increasing the maximum tensile force that the gripper can sustain in its stable state. Consequently, tensile springs with higher tension can be employed, resulting in a faster grasping speed.

1) Fully Active Grasping Mode (FAGM): The FAGM refers to the operational process where the opening and closing of the gripper are entirely controlled by the motion of the pneumatic cylinder's piston rod throughout the entire grasping task. In this mode, the zero position of the moving block is defined when it is in close contact with Electromagnet A at the front end, while the final position is defined when the distance between the moving block and Electromagnet A reaches 20 mm. When the moving block is at the zero position, the BMA gripper is in its fully open state, and when the moving block is at the final position, the gripper is in its fully closed state. As shown in Fig. 6(a), throughout the operation process in the FAGM, Electromagnet A remains de-energized, while Electromagnet B is continuously energized with a voltage set to 5 V, ensuring a magnetic connection between the piston rod and the rear iron

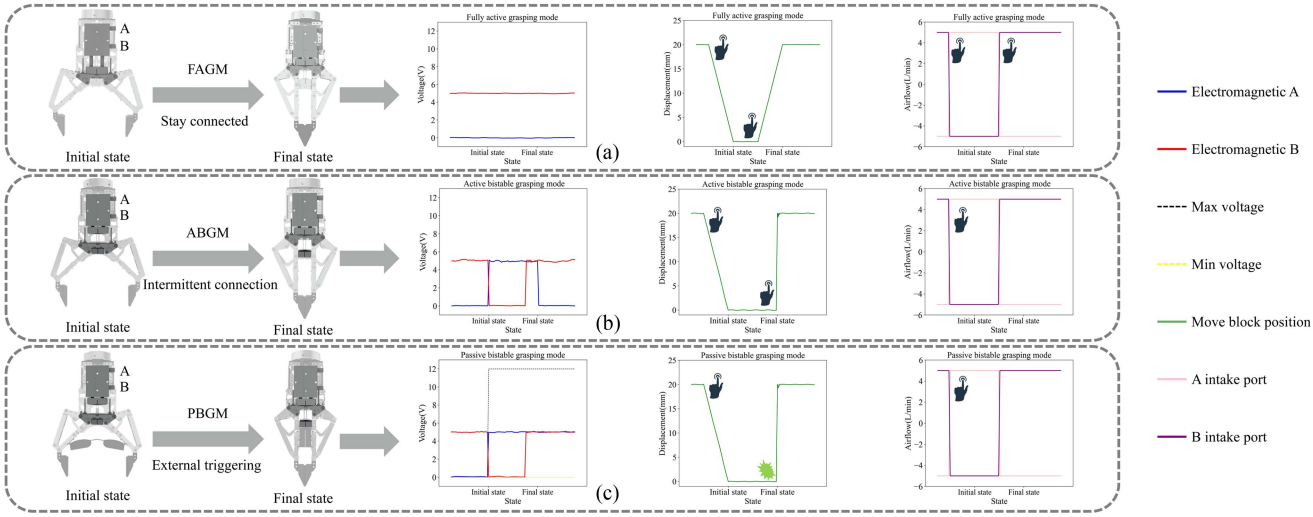

Fig. 6. Schematic diagrams of the BMA gripper operating in three working modes, illustrating the relationships between the voltage variations of Electromagnets A and B, pneumatic input changes, and the positional changes of the moving block. (a) FAGM. (b) ABGM. (c) PBGM.

plate of the moving block. During the preparation phase, the solenoid valve is energized, and airflow from the air pump enters through Port A, with Port B open to the external environment. The piston rod extends, moving the moving block to the zero position, causing the gripper to fully open, corresponding to the initial state shown in Fig. 6(a). During the grasping phase, the solenoid valve is de-energized, and airflow enters through Port B, while Port A is connected to the external environment. The piston rod retracts, driving the moving block to the final position, causing the gripper to close and complete the grasping task, corresponding to the final state in Fig. 6(a). Furthermore, the opening and closing speeds of the gripper can be adjusted by controlling the airflow rate at Ports A and B of the pneumatic cylinder, effectively simulating motor-driven control through the pneumatic system.

2) Active Bistable Grasping Mode (ABGM): The ABGM utilizes a bistable structure to achieve ultra-fast gripper closure, with the timing of closure actively controllable. As shown in Fig. 6(b), in the preparation stage, Electromagnet B is activated while Electromagnet A is deactivated. Simultaneously, the solenoid valve is energized, directing airflow into the pneumatic cylinder through port A while exhausting through port B. The piston rod extends forward, pushing the moving block to the zero position and fully opening the gripper. Subsequently, Electromagnet A is energized and Electromagnet B deactivated, magnetically locking the moving block to Electromagnet A. Next, the solenoid valve is turned-OFF, airflow enters through port B and exhausts from port A, retracting the piston rod; however, the moving block remains secured by Electromagnet A, emulating the latch-lock mechanism of the zebra mantis shrimp's hunting appendage, thereby establishing the first stable state. At this point, Electromagnet B is reactivated. When active triggering for grasping is required, Electromagnet A is deactivated, causing the moving block to disengage from Electromagnet A, thus releasing the latch. Driven rapidly backward by tension springs on both sides, the moving block converts stored elastic potential energy into kinetic energy, quickly closing the gripper to achieve grasping and transitioning to the second stable state, as shown in the final state in Fig. 6(b).

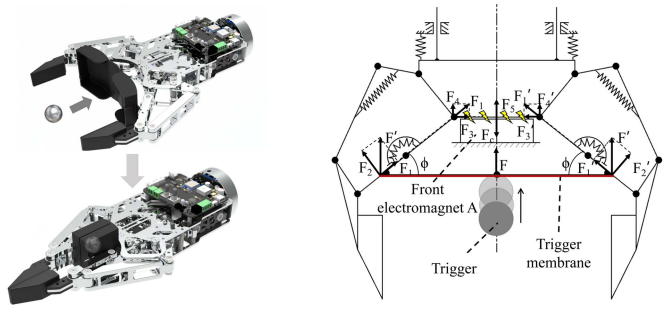

Fig. 7. Schematic diagram illustrating the trigger mechanism of under-actuated link closure in PBGM.

3) Passive Bistable Grasping Mode (PBGM): The PBGM is developed based on the ABGM by installing a trigger membrane between the gripper fingers, allowing the gripper to passively sense external stimuli and trigger closure without active control. As shown in Fig. 6(c), the preparation phase for the passive mode is identical to the active mode. When the trigger membrane receives sufficient external force, it transmits the force to the moving block, causing it to disengage from Electromagnet A. This action overcomes the energy barrier, resulting in the rapid backward movement of the block driven by the tensile spring, thereby closing the gripper.

As shown in Fig. 7, in this mode, the open state of the gripper is maintained by the combined magnetic forces of permanent magnets and front-end Electromagnet A, keeping the trigger membrane in a tightened state. Since the collision between the object and the trigger membrane occurs instantaneously, the membrane can be regarded as rigid at this moment. The collision-induced impact force F is transmitted to the moving

block through the linkage mechanism of the gripper, and this force transmission relationship can be expressed as follows:

$$F_1 = F_1' = \frac{F}{2}\sin\phi$$
$$F_4 = F_4' = F_1\sin\phi$$
$$F_5 = F_4 + F_4'. \tag{7}$$

The simplified transmission yields the force F_5, which is transmitted to the moving block to overcome the magnetic force F_C for detachment, as follows:

$$F_5 = F \cdot \sin^2\phi. \tag{8}$$

To prevent unintended triggering caused by nontarget stimuli—such as minor disturbances when the target is a stone rather than sand—the gripper must possess the capability to adjust its response threshold to external stimuli, thereby filtering out unintentional activations. In this device, programmable control of the gripper's trigger sensitivity is achieved by adjusting the voltage applied to Electromagnet A. According to the fundamental principles of electromagnetism and Ampère's law, the magnetic force generated by the electromagnet can be expressed as

$$F_c = \frac{(N \cdot I)^2 \cdot \mu_0 \cdot A}{2 \cdot g^2} \tag{9}$$

where F_c is the magnetic force (N), N is the number of coil turns, I is the current through the coil (A), μ_0 is the vacuum permeability, A is the cross-sectional area of the iron core (m^2), and g is the gap distance between the electromagnet and the attracted object (m). By incorporating Ohm's law to relate current with voltage and resistance, the equation can be further expressed as

$$F_c = \frac{N^2 \cdot U^2 \cdot \mu_0 \cdot A}{2 \cdot R^2 \cdot g^2}. \tag{10}$$

Here, U is the input voltage (V), and R is the coil resistance (Ω). Since Electromagnet A is energized for a short duration, the temperature rises and its effect on resistance can be neglected. During the attraction process, parameters n, μ_0, A, and g are considered constant, resulting in a positive correlation between magnetic force and input voltage. The voltage adjustment range in the device is set from 0 to 12 V. By varying the input voltage, the magnetic force can be controlled, thereby adjusting the gripper's response threshold to external stimuli, enabling programmable sensitivity control without altering the mechanical structure.

III. Experimental Verification

In this section, we conduct experimental validation to evaluate the performance and functionality of the BMA gripper. The overall parameters of the BMA gripper are listed in Table I.

A. Rapid Grasping Experiment Under Diverse Conditions

BMA gripper, as a device that leverages bistability and possesses grasping adaptability, is capable of rapid grasping under various conditions. As shown in Fig. 8, four grasping scenarios were designed, and six common objects—namely a Rubik's Cube, a spherical object, a duck toy, a cardboard box, a picture frame, a beverage bottle, and a whiteboard eraser—were selected for testing. In both the FAGM and the ABGM, 50 grasping trials were performed for each object and the success rates were recorded. Specifically, Fig. 8(a) corresponds to the case in Fig. 4(a) where the object is too far in the vertical direction and barely contacted, Fig. 8(b) corresponds to the narrow-space grasping scenario in Fig. 4(b), Fig. 8(c) corresponds to the case in Fig. 4(c) where the object is too close in the vertical direction and in contact with the ground, and Fig. 8(d) corresponds to the grasping of objects with irregular shapes or significant height, as shown in Fig. 4(d).

Experimental results indicate that the BMA gripper achieves a minimum grasping success rate of 82% under all four conditions. Although the FAGM mode exhibits slightly slower grasping speeds, it offers higher stability and success rates, whereas the ABGM mode enables ultrafast grasping but generates considerable kinetic energy during bistable state transitions, which may impart significant impact on the objects and consequently reduce

TABLE I
BMA Gripper Overall Performance Parameters

Items	Parameters
Weight	1.035 kg
Dimension (H × L × W)	293 mm × 211 mm × 42 mm (Open state) 306 mm × 143 mm × 42 mm (Closed state)
Driving source	Cylinder × 1 Electromagnet × 2
Compressed air	0 – 0.4 MPa
Voltage regulation range	0 – 12 V
Total stroke	140 mm
Fastest closing time	0.116 s
Minimum triggering energy	0.412 mJ
Maximum power	120 Watt
MCU	STM32G431C8T6
Fingertip type	Ordinary fingertip Flat object fingertip

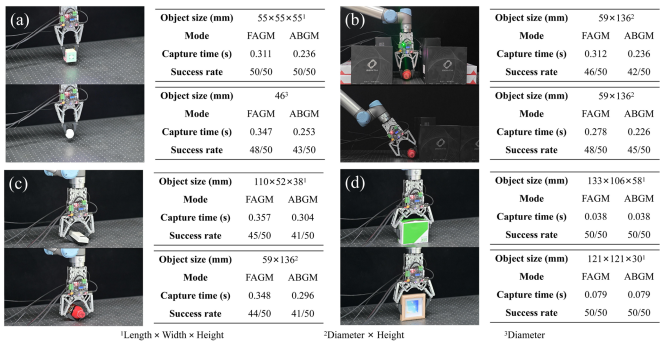

Fig. 8. Rapid grasping experiment under diverse conditions. (a) Grasping under vertical collision with the ground, with target objects being a beverage bottle and a whiteboard eraser. (b) Grasping by fingertip extension, with target objects being a Rubik's cube and a spherical object. (c) Grasping under horizontal compression with a wall surface, with the target object being a beverage bottle. (d) Grasping under conditions of collision with internal objects, with target objects being a paper box and a photo frame.

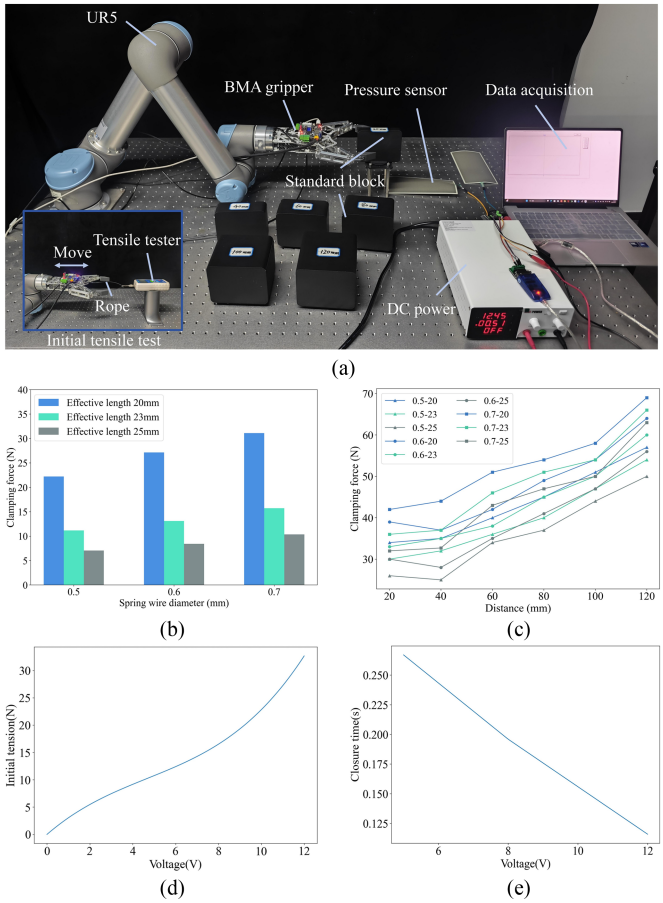

Fig. 9. Experimental evaluation of the reprogrammable capability of the BMA gripper using different elastic potential energy components. (a) Experimental setup for measuring initial tensile force, gripping force, required voltage of Electromagnet A, and closure time for various elastic components (the tension springs used are listed in Table II). (b) Relationship between initial tensile force and the nine tension springs. (c) Gripping force of the nine tension springs under different gripping distances. (d) Relationship between voltage of Electromagnet A and initial tensile force. (e) Relationship between voltage of Electromagnet A and closure time.

the success rate. In practical applications, the grasping mode can be selected according to specific requirements.

B. Experiment on Reprogrammable Capability Verification

In order to verify the reprogrammable capability of the proposed BMA gripper, we set up an experimental platform, as shown in Fig. 9(a). Tests were conducted on the initial tension of tension springs with different lengths and wire diameters, the gripping force under different gripping distances, and the initial tension and closing time corresponding to different voltages of the front electromagnet A. In this experiment, we connected a tension tester to the moving block of the BMA gripper and replaced different tension springs to measure the force required to maintain the gripper jaws in the open state. As shown in Fig. 9(b), it can be observed that larger spring wire diameters and shorter effective lengths store higher levels of bistable energy,

TABLE II
PARAMETERS OF TENSION SPRING STEEL BALL

Wire diameter (mm)	Length (mm)	Diameter (mm)	Weight (g)
0.5	20,23,25	12.7	8.36
0.6	20,23,25	18	4.09
0.7	20,23,25	8	2.06
/	/	6	1.05

thus requiring greater force to keep the jaws open. Meanwhile, as the stored bistable energy increases, once the latch is released, the jaws close more rapidly, resulting in higher gripping forces at the same gripping distance.

On the other hand, six different standard blocks with gripping widths of 20, 40, 60, 80 100, and 120 mm were selected, and flexible film pressure sensors were attached to the contact surfaces of these blocks to measure the gripping force. As shown in Fig. 9(c), among the six gripping distances tested, replacing different elastic potential energy components allowed the jaws to achieve a maximum gripping force of 68.4 N, corresponding to an initial tension of 32.4 N. When the gripping distance is relatively small (e.g., 20 mm), the magnetic force of the front electromagnet A provides additional enhancement, causing the gripping force at 20 mm to be similar to that at 40 mm. Fig. 9(d) shows the relationship between initial tension and the voltage of the front electromagnet A. To maintain the jaws in the open state, as the BMA gripper's stored energy increases, the force required to keep the latch closed—adjusted by the front electromagnet A's magnetic force—must also increase. Fig. 9(e) presents the closing time curves under the ultrasensitive state for different voltages of the front electromagnet A, indicating that the shortest closing time can reach 0.116 s. As the voltage decreases, the energy that can be accommodated also decreases, and thus the closing time becomes correspondingly longer. These experimental results demonstrate that by replacing the elastic potential energy components and adjusting the voltage of the front electromagnet A, the BMA gripper can be reprogrammed to meet different gripping requirements, thereby showcasing its excellent reprogrammable capability.

C. Selective Passive Trigger Grasping Experiment

To intuitively demonstrate the reprogrammable capability of the BMA gripper under the PBGM, an experimental platform was established to evaluate its performance in selective grasping, as shown in Fig. 10. Initially, the gripper was maintained in its initial state, and the voltage of Electromagnet A at the front end was adjusted to 12 V, 8 V, and 5 V, respectively. Subsequently, four steel balls of varying sizes and weights (as detailed in Table II) were dropped from the same height and position to provide external stimuli of different magnitudes to the trigger membrane of the BMA gripper, in an attempt to initiate the bistable state transition. When the voltage was set to 12 V, the BMA gripper was in its lowest sensitivity state, and the 10 mm steel ball failed to provide sufficient stimulus to overcome the energy barrier and trigger the grasp. However, when replaced with a 12.7 mm steel ball, the stimulus was sufficient to trigger

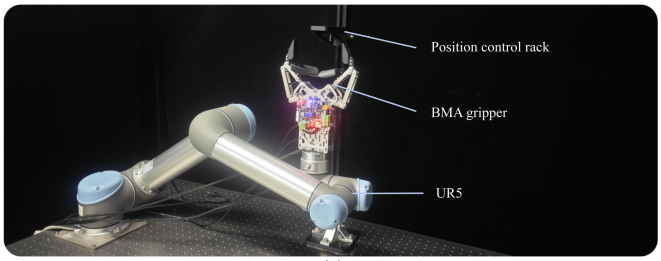

(a)

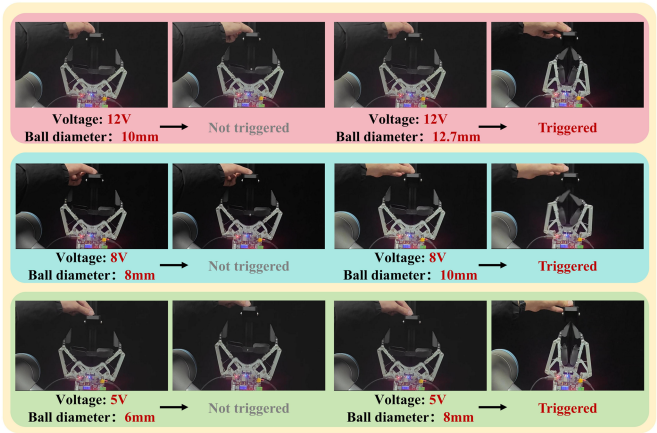

(b)

Fig. 10. Selective passive-triggered grasping experiments. (a) Experimental setup: the height and position of the steel ball relative to the trigger membrane are fixed by a position control frame, and passive grasping tests are conducted with the steel ball weight (magnitude of external stimulus) as the variable (steel ball parameters are listed in Table II). (b) Reprogramming the trigger sensitivity by adjusting the voltage supplied to Electromagnet A, enabling the BMA gripper to selectively grasp objects under different stimulus intensities (examples shown at voltages of 12 V, 8 V, and 5 V).

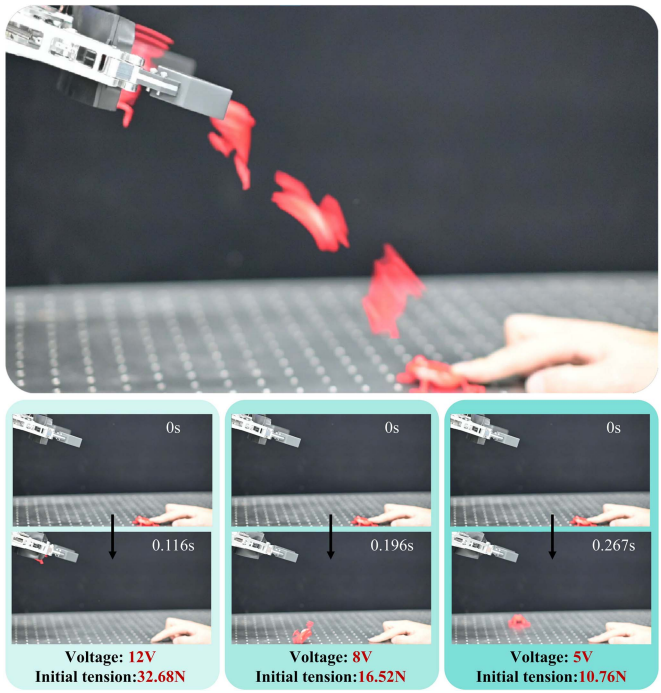

Fig. 11. High-dynamic object grasping demonstration of BMA gripper. In the passive bistable triggering mode under three different voltage settings, the elastic component fixed to the moving block was adjusted to achieve an ultrasensitive state at each voltage level, enabling the capture of a jumping frog toy. The dimensions of the jumping frog are 37 × 42 × 17 mm.

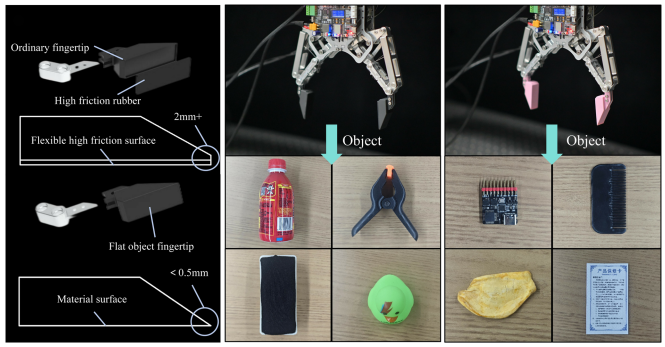

(a) (b) (c)

Fig. 12. Modular fingertip structures and demonstration of grasped objects. (a) Comparison of structural differences between flat-object fingertips and standard fingertips. (b) Standard fingertips, used for grasping objects of regular shapes and sizes, such as beverage bottles, shelves, whiteboard erasers, and rubber duck toys. (c) Flat-object fingertips, designed for grasping thin objects, such as mini debuggers, combs, dried sweet potatoes, and cards.

the state transition and complete the grasp. The voltage was then reprogrammed to 8 V and 5 V for subsequent tests. The experimental results indicated that the sensitivity increased as the voltage decreased, allowing smaller external stimuli (i.e., smaller steel balls) to successfully trigger the state transition. This experiment demonstrates that the PBGM of the proposed BMA gripper can be preprogrammed to possess different sensitivity levels, enabling it to establish varied energy barriers and selectively respond to objects providing different stimulus magnitudes.

D. Highly Dynamic Object Grasping Experiment

The zebra mantis shrimp can capture moving prey at remarkable speeds. To validate that the proposed BMA gripper can achieve similar high-dynamic object capture capabilities, we conducted a series of experiments using jumping frogs, as shown in Fig. 11. Initially, the gripper was set to the default PBGM, with the voltage of front Electromagnet A set to 5 V. The bistable spring element was adjusted to enable BMA gripper's fastest closing and ultra-sensitive state at this voltage, with a tested initial pulling force of 10.76 N using a dynamometer. When the jumping frog impacted the trigger membrane, the gripper entered state transition, but the frog exited the capture range before the jaws closed, despite the closing occurring within 0.267 s.

The voltage was then adjusted to 8 V, maintaining the fastest closing and ultra-sensitive state at this setting, yielding an initial pulling force of 16.52 N with a closing time of 0.196 s, yet capture was still unsuccessful. Finally, we set the voltage to 12 V, achieving an initial pulling force of 32.68 N in its fastest, ultra-sensitive state. Experimental results showed that the jaws

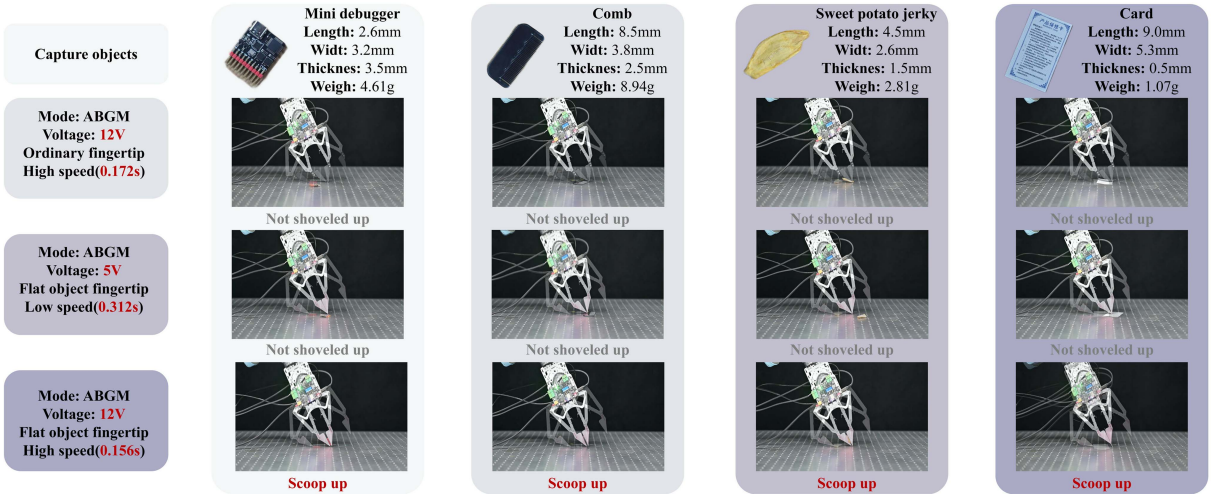

Fig. 13. Testing the scooping capability of the BMA gripper's modular flat-object fingertips for flat objects. Under the ABGM, the BMA gripper was tilted at a 50° angle relative to the ground. Three sets of comparative experiments were conducted with controlled parameters. The scooped objects, arranged from left to right, include a mini debugger, a comb, a dried sweet potato slice, and a card, with thicknesses decreasing in order.

closed within 0.116 s, successfully capturing the jumping frog. This experiment demonstrates the critical role of BMA gripper's reprogrammable functionality in high-dynamic object grasping, allowing it to autonomously adjust trigger sensitivity and jaw closing speed according to task requirements, significantly reducing algorithmic complexity in dynamic object capture.

E. Modular Fingertip Functional Verification

In this study, two types of modular fingertips were designed for the BMA gripper: standard fingertips and flat-object fingertips. As shown in Fig. 12(a), the standard fingertips are equipped with flexible high-friction rubber pads made of 75 A rubber on their surfaces. These pads provide significant friction during grasping, enhancing the gripper's ability to hold heavier objects. However, due to the inherent thickness of the rubber pads, the fingertip ends require a certain thickness (2 mm in this study). This thickness limits the fingertips' ability to scoop up flat objects, making them more suitable for grasping objects of regular shapes and sizes, as shown in Fig. 12(b).

To address this limitation, flat-object fingertips were designed with an end thickness of less than 0.5 mm. However, the reduced thickness means the surface is limited to the base material of the fingertips, resulting in lower friction compared to the standard fingertips. Nonetheless, they are better suited for grasping thinner and lighter objects, as shown in Fig. 12(c). The grasping performance of the standard fingertips has been discussed earlier. Therefore, the following section will focus on testing the scooping capability of the flat-object fingertips for flat objects.

To evaluate the scooping capability of the flat-object fingertip, three experimental setups were designed, as shown in Fig. 13:

1) high-speed and conventional fingertip;
2) low-speed and flat-object fingertip; and
3) high-speed and flat-object fingertip.

In the first set of experiments, the BMA gripper operated in an ultra-sensitive state at 12 V, with a closing time of approximately 0.172 s. However, when using the conventional fingertip, the gripper was unable to reliably scoop thin sheets, only sporadically scooping the thickest mini debugger, with a success rate of about 10%. In the second set, the BMA gripper was set to an ultra-sensitive state at 5 V, with a closing time of approximately 0.312 s. Despite switching to the flat-object fingertip, the gripper still failed to reliably scoop thin sheets—even with the thickest mini debugger. It was not until the third set, where the BMA gripper operated in an ultra-sensitive state at 12 V with a closing time of approximately 0.156 s and employed the flat-object fingertip, that all four thicknesses of thin sheets could be successfully scooped, achieving an average success rate of over 90% over 50 trials. These results demonstrate that, in the active bistable mode, the BMA gripper combined with the flat-object fingertip can efficiently perform the task of scooping thin sheets with a thickness of up to 0.5 mm—a task that is challenging to accomplish with conventional grippers or those relying solely on ultra-fast actuation and a fixed fingertip design.

IV. Conclusion

Inspired by the physiological structure and predation mechanisms of the zebra mantis shrimp, this study proposes a bioinspired gripper, named the BMA gripper, which incorporates active, active bistable, and PBGMs. The BMA gripper also adopts a modular fingertip design capable of performing specialized tasks, such as scooping flat objects, significantly expanding its applicability. Future work may further diversify fingertip configurations to enhance adaptability to various tasks.

To demonstrate the novelty and superiority of the BMA gripper, extensive experiments were conducted under different grasping conditions. Results indicated that the device can achieve rapid bistable transitions within only 0.116 s in passive bistable mode, effectively addressing the longstanding challenge of simultaneously achieving high speed and adaptability in grasping mechanisms.

This work broadens the application scope of bistability in robotic grasping. Although the BMA gripper demonstrates promising functionality and potential, further optimizations remain possible. First, sensitivity reprogramming currently depends on voltage adjustment, potentially causing overheating issues with prolonged high-voltage use. Second, repeated use of elastic components may cause fatigue, requiring frequent replacements, prompting future exploration of alternative elastic elements. Finally, despite the validations of multimode, high-speed, and high-sensitivity grasping performance and promising application scenarios, further research directions, such as underwater and space exploration, remain to be explored.

REFERENCES

[1] J. Shintake, V. Cacucciolo, D. Floreano, and H. Shea, "Soft robotic grippers," *Adv. Mater.*, vol. 30, no. 29, 2018, Art. no. 1707035.

[2] J. Langowski, P. Sharma, and A. L. Shoushtari, "In the soft grip of nature," *Sci. Robot.*, vol. 5, no. 49, 2020, Art. no. eabd9120.

[3] Y. Sun, Y. Liu, F. Pancheri, and T. C. Lueth, "LARG: A lightweight robotic gripper with 3-D topology optimized adaptive fingers," *IEEE/ASME Trans. Mechatron.*, vol. 27, no. 4, pp. 2026–2034, Aug. 2022.

[4] X. Chen et al., "WebGripper: Bioinspired cobweb soft gripper for adaptable and stable grasping," *IEEE Trans. Robot.*, vol. 39, no. 4, pp. 3059–3071, Aug. 2023.

[5] R. Sachse et al., "Snapping mechanics of the venus flytrap (Dionaea Muscipula)," *Proc. Nat. Acad. Sci.*, vol. 117, no. 27, pp. 16035–16042, 2020.

[6] M. Smith, G. Yanega, and A. Ruina, "Elastic instability model of rapid beak closure in hummingbirds," *J. Theor. Biol.*, vol. 282, no. 1, pp. 41–51, 2011.

[7] F. Haas, S. Gorb, and R. J. Wootton, "Elastic joints in dermapteran hind wings: Materials and wing folding," *Arthropod Struct. Develop.*, vol. 29, no. 2, pp. 137–146, 2000.

[8] E. Steinhardt et al., "A physical model of mantis shrimp for exploring the dynamics of ultrafast systems," *Proc. Nat. Acad. Sci.*, vol. 118, no. 33, 2021, Art. no. e2026833118.

[9] J. A. Faber, A. F. Arrieta, and A. R. Studart, "Bioinspired spring origami," *Science*, vol. 359, no. 6382, pp. 1386–1391, 2018.

[10] T. Jin et al., "Origami-inspired soft actuators for stimulus perception and crawling robot applications," *IEEE Trans. Robot.*, vol. 38, no. 2, pp. 748–764, Apr. 2022.

[11] D. Tang et al., "Bistable soft jumper capable of fast response and high takeoff velocity," *Sci. Robot.*, vol. 9, no. 93, 2024, Art. no. eadm8484.

[12] N. Hou et al., "Reticular origami soft robotic gripper for shape-adaptive and bistable rapid grasping," *Soft Robot.*, vol. 11, pp. 550–560, 2024.

[13] C. Wang, H. Guo, R. Liu, Z. Deng, Y. Chen, and Z. You, "Reconfigurable origami-inspired multistable metamorphous structures," *Sci. Adv.*, vol. 10, no. 22, 2024, Art. no. eadk8662.

[14] H. Zhang, E. Lerner, B. Cheng, and J. Zhao, "Compliant bistable grippers enable passive perching for micro aerial vehicles," *IEEE/ASME Trans. Mechatron.*, vol. 26, no. 5, pp. 2316–2326, Oct. 2021.

[15] Q. Qi, C. Xiang, V. A. Ho, and J. Rossiter, "A sea-anemone-inspired, multifunctional, bistable gripper," *Soft Robot.*, vol. 9, no. 6, pp. 1040–1051, 2022.

[16] Z. Chen, J. Sun, and J. Zhao, "Tuning modules with elastic instabilities on-the-fly for reconfigurable shapes and motions," *IEEE/ASME Trans. Mechatron.*, vol. 29, no. 4, pp. 3117–3127, Aug. 2024.

[17] Y. Jiang et al., "Reprogrammable bistable actuators for multimodal, fast, and ultrasensitive grasping," *IEEE/ASME Trans. Mechatron.*, vol. 29, no. 2, pp. 984–994, Apr. 2024.

[18] L. Jiang, B. Li, F. Ma, and G. Chen, "A tristable actuator for a bidirectional crawling and falling-rebootable robot," *IEEE/ASME Trans. Mechatron.*, vol. 29, no. 2, pp. 856–865, Apr. 2024.

[19] P. Zhang and B. Tang, "A two-finger soft gripper based on bistable mechanism," *IEEE Robot. Autom. Lett.*, vol. 7, no. 4, pp. 11330–11337, Oct. 2022.

[20] J.-S. Koh et al., "Jumping on water: Surface tension–dominated jumping of water striders and robotic insects," *Science*, vol. 349, no. 6247, pp. 517–521, 2015.

[21] R. Wang, J. Wang, Z. Zhu, and D. Wang, "Multimodal magnetic soft robots enabled by bistable kirigami patterns," *IEEE/ASME Trans. Mechatron.*, vol. 29, no. 6, pp. 4526–4537, Dec. 2024.

[22] Y. Liu et al., "A soft and bistable gripper with adjustable energy barrier for fast capture in space," *Soft Robot.*, vol. 10, no. 1, pp. 77–87, 2023.

[23] A. Pal, D. Goswami, and R. V. Martinez, "Elastic energy storage enables rapid and programmable actuation in soft machines," *Adv. Funct. Mater.*, vol. 30, no. 1, 2020, Art. no. 1906603.

[24] R. Antunes, L. Lang, M. L. de Aguiar, T. Assis Dutra, and P. D. Gaspar, "Design of fin ray effect soft robotic gripper for improved mechanical performance and adaptability: Numerical simulations and experimental validation," in *Proc. 20th IEEE/ASME Int. Conf. Mechatronic Embedded Syst. Appl.*, 2024, pp. 1–6.

[25] S.-J. Park, H.-J. Jeon, J.-H. Meng, and J.-B. Song, "Gripper with adaptability to environmental constraints," *IEEE Robot. Autom. Lett.*, vol. 9, no. 7, pp. 6608–6615, Jul. 2024.

[26] G. Chen et al., "Design and control of a novel bionic mantis shrimp robot," *IEEE/ASME Trans. Mechatron.*, vol. 28, no. 6, pp. 3376–3385, Dec. 2023.

[27] F. Ito, Y. Ishii, S. Kurumaya, K. Kagaya, and T. Nakamura, "Instantaneous force generation mechanism based on the striking motion of mantis shrimp—Design and control method of cavitation by simulation and experiment," *IEEE Robot. Autom. Lett.*, vol. 7, no. 4, pp. 9342–9349, Oct. 2022.

[28] F. Ito, Y. Ishii, S. Kurumaya, K. Kagaya, and T. Nakamura, "A design method for instantaneous force generation based on a mantis shrimp with exoskeleton spring," *IEEE/ASME Trans. Mechatron.*, vol. 29, no. 2, pp. 960–971, Apr. 2024.

[29] S. C. Wells, N.-S. P. Hyun, E. Steinhardt, T. H. Nguyen, and R. J. Wood, "Design optimization of an ultrafast-striking mantis shrimp microrobot," in *Proc. IEEE/RSJ Int. Conf. Intell. Robots Syst.*, 2022, pp. 4236–4242.

[30] S. N. Patek, W. Korff, and R. L. Caldwell, "Deadly strike mechanism of a mantis shrimp," *Nature*, vol. 428, no. 6985, pp. 819–820, 2004.

Tao Liao received the B.E. degree in mechanical design, manufacturing, and automation from South China Agricultural University, Guangzhou, China, in 2023. He is currently working toward the M.S. degree in electronic information with Tsinghua Shenzhen International Graduate School, Tsinghua University, Shenzhen, China.

His research interests include robotics, mechanical arm, manipulators, and gripper.

Houde Liu received the B.S. degree in automation from the Huazhong University of Science and Technology, Wuhan, China, in 2007, and the M.S. and Ph.D. degrees in control science and engineering from the Harbin Institute of Technology, Harbin, China, in 2009 and 2013, respectively.

He is currently a Full Professor with the Centre for Artificial Intelligence and Robotics, Tsinghua Shenzhen International Graduate School, Tsinghua University, Beijing, China. His research interests include space robots, motion planning and control.

Chongkun Xia (Member, IEEE) received the Ph.D. degree in pattern recognition and intelligent systems from Northeastern University, Shenyang, China, in 2021.

In the past years, he was a postdoc with the Centre for Artificial Intelligence and Robotics, Tsinghua University, Beijing, China. He is currently an Associate Professor and a Leader with the Robot Technology and Intelligent Perception Group, School of Advanced Manufacturing, Sun Yat-Sen University, Guangzhou, China. His research interests include robotics, motion planning, and machine learning.

Shoujie Li (Member, IEEE) received the B.Eng. degree in electronic information engineering from the College of Oceanography and Space Informatics, China University of Petroleum, Tsingtao, China, in 2020. He is currently working toward the Ph.D. degree with the Tsinghua-Berkeley Shenzhen Institute, Shenzhen International Graduate School, Tsinghua University, Shenzhen, China.

His research interests include tactile perception, grasping, and machine learning.

Dr. Li was the recipient of the Outstanding Mechanisms and Design Paper Finalists in ICRA 2022 and the Best Application Paper Finalists in IROS 2023. He was also the recipient of first place in the Robotic Grasping of Manipulation Competition-Picking in Clutter in ICRA 2024.

Xueqian Wang (Member, IEEE) received the Ph.D. degree in control science and engineering from the Harbin Institute of Technology, Harbin, China, in 2010.

He is currently a Professor and the Leader with the Center of Intelligent Control and Telescience, Tsinghua Shenzhen International Graduate School, Tsinghua University, Shenzhen, China. His research interests include dynamics modeling, control, and teleoperation of robotic systems.

Bin Liang (Senior Member, IEEE) received the Ph.D. degree in mechanical automation from the Department of Precision Instrument, Tsinghua University, Beijing, China, in 1994.

Since 2007, he has been a Professor with the Department of Automation, Tsinghua University. His research interests include modeling and control of dynamic systems.